

Original Research Article

**MHD Free Convection, Heat and Mass Transfer
with Chemical Reaction, Radiation and Heat
Source or Sink over a Rotating Inclined
Permeable Plate with Variable Reactive Index**

ABSTRACT

MHD free convection, heat and mass transfer flow over a rotating inclined permeable plate with the influence of magnetic field, thermal radiation and chemical reaction of various order has been investigated numerically. The steady laminar boundary layer flow is considered in this study. The governing boundary-layer equations are formulated and transformed into a set of similarity equations with the help of similarity variables derived by lie group transformation. The governing equations are solved numerically using the Nactsheim-Swigert Shooting iteration technique together with the Runge-Kutta six order iteration schemes with the help of a computer programming language Compaq Visual Fortran 6.6a. The simulation results are presented graphically to illustrate influence of magnetic parameter (M), porosity parameter (γ), rotational parameter (R'), Grashof number (G_r), modified Grashof number (G_m), thermal conductivity parameter (T_c), Prandtl number (P_r), radiation parameter (R), heat source parameter (Q), Eckert number (E_c), Schmidt number (S_c), reaction parameter (λ) and order of chemical reaction (n) on the all fluid velocity components, temperature and concentration distribution as well as Skin-friction coefficient, Nusselt and Sherwood number at the plate.

MHD

Keywords: ~~Free convection; Heat and mass transfer; Inclined permeable plate; Thermal radiation; Chemical reaction; Lie group transformation; Nactsheim-Swigert Shooting iteration technique; Runge-Kutta six order iteration schemes.~~

NOMENCLATURE

B_0	Constant magnetic flux density
c	Constant depends on the properties of the fluid
C	Concentration of the fluid
C_p	Specific heat at constant pressure
D_m	Mass diffusivity
f'	Dimensionless primary velocity
g	Acceleration due to gravity
g_0	Dimensionless secondary velocity

26	k	Thermal conductivity
27	k_{∞}	Undisturbed thermal conductivity
28	k_0	Reaction rate
29	K	Permeability of the porous medium
30	n	Order of chemical reaction
31	P	Pressure distribution in the boundary layer
32	q_r	Radiative heat flux in the y direction
33	Q_T	Heat generation
34	Q_0	Heat source
35	t	Time
36	T	Fluid temperature
37	U	Uniform velocity
38	u, v	Velocity components along x and y axes respectively
39	x'	Dimensionless axial distance along x axis

40 **Dimensionless parameters**

41	E_c	Eckert number
42	R'	Rotational parameter
43	G_r	Grashof number
44	G_m	Modified Grashof number
45	M	Magnetic parameter
46	P_r	Prandtl number
47	Q	Heat source parameter
48	R	Radiation parameter
49	S_c	Schmidt number
50	T_c	Thermal conductivity parameter
51	γ	Permeability of the porous medium
52	λ	Reaction parameter

53

54 **Greek Symbols**

55	ν	Kinematic viscosity of the fluid
56	μ	Dynamic viscosity of the fluid

57	σ	Electrical conductivity
58	σ_0	Constant electrical conductivity
59	σ_s	Stefan-Boltzmann constant
60	ρ	Density of the fluid
61	α	Thermal diffusivity
62	$\alpha_1 - \alpha_6$	Arbitrary real number
63	β	Inclination angle
64	β_T	Thermal expansion coefficient
65	β_c	Concentration expansion coefficient
66	κ^*	Mean absorption coefficient
67	ε	Parameter of the group
68	ψ	Stream function
69	η	Similarity variable
70	θ	Dimensionless temperature
71	ϕ	Dimensionless concentration
72	Ω	Angular velocity of the plate
73	Subscripts	
74	w	Condition of the wall
75	∞	Condition of the free steam

1. INTRODUCTION

Coupled heat and mass transfer problems in presence of chemical reactions are of importance in many processes and have, therefore, received considerable amount of attention of researchers in recent years. Chemical reactions can occur in processes such as drying, distribution of temperature and moisture over agricultural fields and groves of fruit trees, damage of crops due to freezing, evaporation at the surface of a water body, energy transfer in a wet cooling tower and flow in a desert cooler. Chemical reactions are classified as either homogeneous or heterogeneous processes. A homogeneous reaction is one that occurs uniformly throughout a given phase. On the other hand, a heterogeneous reaction takes a restricted area or within the boundary of a phase. Analysis of the transport processes and their interaction with chemical reactions is quite difficult and closely related to fluid dynamics. Chemical reaction effects on heat and mass transfer has been analyzed by many researchers over various geometries with various boundary conditions in porous and nonporous media. Symmetry groups or simply symmetries are invariant transformations that do not alter the structural form of the equation under investigation which is described by Bluman and Kumei [1]. MHD boundary layer equations for power law fluids with variable electric conductivity is studied by Helmy [2]. In the case of a scaling group of

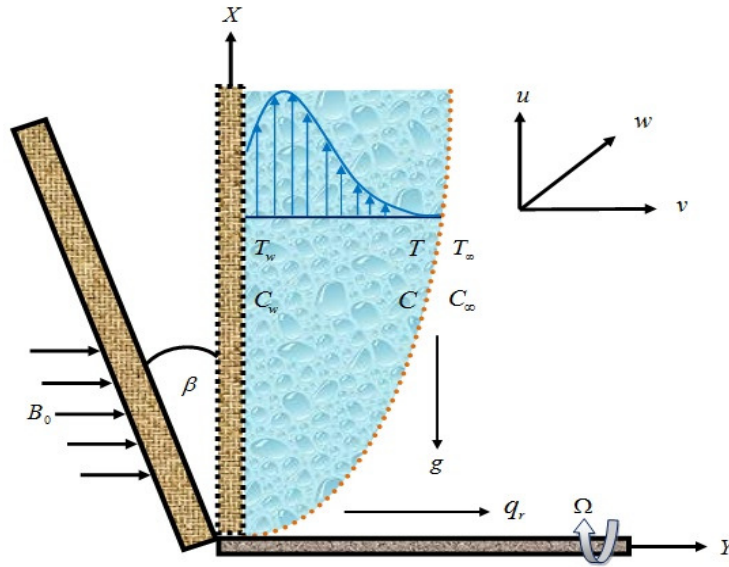
transformations, the group-invariant solutions are nothing but the well known similarity solutions which is studied by Pakdemirli and Yurusoy [3]. Symmetry groups and similarity solutions for free convective boundary-layer problem was studied by Kalpakides and Balassas [4]. Makinde [5] investigated the effect of free convection flow with thermal radiation and mass transfer past moving vertical porous plate. Seddeek and Salem [6] investigated the Laminar mixed convection adjacent to vertical continuously stretching sheet with variable viscosity and variable thermal diffusivity. Ibrahim, Elaiw and Bakr [7] studied the effect of the chemical reaction and radiation absorption on the unsteady MHD free convection flow past a semi infinite vertical permeable moving plate with heat source and suction. El-Kabeir, El-Hakiem and Rashad [8] studied Lie group analysis of unsteady MHD three dimensional dimensional by natural convection from an inclined stretching surface saturated porous medium. Rajeswari, Jothiram and Nelson [9] studied the effect of chemical reaction, heat and mass transfer on nonlinear MHD boundary layer flow through a vertical porous surface in the presence of suction. Chandrakala [10] investigated chemical reaction effects on MHD flow past an impulsively started semi-infinite vertical plate. Joneidi, Domairry and Babaelahi [11] studied analytical treatment of MHD free convective flow and mass transfer over a stretching sheet with chemical reaction. Muhaimin, Kandasamy and Hashim [12] studied the effect of chemical reaction, heat and mass transfer on nonlinear boundary layer past a porous shrinking sheet in the presence of suction. Rahman and Salahuddin [13] studied hydromagnetic heat and mass transfer flow over an inclined heated surface with variable viscosity and electric conductivity. As per standard text and works of previous researchers, the radiative flow of an electrically conducting fluid and heat and mass transfer situation arises in many practical applications such as in electrical power generation, astrophysical flows, solar power technology, space vehicle re-entry, nuclear reactors.

The objective of this study is to present a similarity analysis of boundary layer flow past a rotating inclined permeable plate with the influence of magnetic field, thermal radiation, thermal conductivity and chemical reaction of various orders. The governing equations are transformed into nonlinear ordinary differential equations which depends on the magnetic parameter, the porosity parameter, rotational parameter, the Grashof number, the modified Grashof number, the thermal conductivity parameter, the radiation parameter, the Prandtl number, the Eckert number, the heat source parameter, the Schmidt number, the reaction parameter and order of the chemical reaction respectively. The obtained non-linear coupled ordinary differential equations are solved numerically using Nactsheim-Swigert shooting technique together with Runge-Kutta six order iteration schemes. The primary velocity, secondary velocity, temperature and concentration distributions are discussed and presented graphically. In addition with the skin-friction coefficient, the surface heat and mass transfer rate at the plate are investigated.

2. MATHEMATICAL MODEL OF THE FLOW AND GOVERNING EQUATIONS

Steady two dimensional MHD heat and mass transfer flow with chemical reaction and radiation over an inclined permeable plate $y = 0$ in a rotating system under the influence of transversely applied magnetic field is considered. The x -axis is taken in the upward direction and y -axis is normal to it. Again the plate is inclined at an angle β with the x -axis. The flow takes place at $y \geq 0$, where y is the coordinate measured normal to the x -axis. Initially we consider the plate as well as the fluid is at rest with the same velocity $U (= U_{\infty})$, temperature $T (= T_{\infty})$ and concentration $C (= C_{\infty})$. Also it is assumed that the fluid and plate is at rest after that the whole system is allowed to rotate with a constant angular velocity $R = (0, -\Omega, 0)$ about the y -axis and then the temperature and species concentration of the

plate are raised to $T_w (> T_\infty)$ and $C_w (> C_\infty)$ respectively, which are thereafter maintained constant, where T_w and C_w is the temperature and concentration respectively at wall and T_∞ and C_∞ is the temperature and concentration respectively far away from the plate.



148
149

150 **Fig. 1. Physical configuration of the flow**

151 The electrical conductivity is assumed to vary with the velocity of the fluid and have the form
152 [2],

153 $\sigma = \sigma_0 u$, σ_0 is the constant electrical conductivity.

154 The applied magnetic field strength is considered, as follows [13]

$$155 \quad B(x) = \frac{B_0}{\sqrt{x}}$$

156 The temperature dependent thermal conductivity is assumed to vary linearly, as follows [6]

$$157 \quad k(T) = k_\infty [1 + c(T - T_\infty)]$$

158 Where k_∞ is the undisturbed thermal conductivity and c is the constant depending on the
159 properties of the fluid.

160 The governing equations for the continuity, momentum, energy and concentration in laminar
161 MHD incompressible boundary-layer flow can be presented, respectively as follows

$$162 \quad \frac{\partial u}{\partial x} + \frac{\partial v}{\partial y} = 0 \quad (1)$$

$$163 \quad u \frac{\partial u}{\partial x} + v \frac{\partial u}{\partial y} = v \frac{\partial^2 u}{\partial y^2} + 2\Omega w - \frac{v}{K} u - \frac{\sigma_0 B_0^2 u^2}{\rho x} + g\beta_T (T - T_\infty) \cos\beta + g\beta_C (C - C_\infty) \cos\beta \quad (2)$$

$$164 \quad u \frac{\partial w}{\partial x} + v \frac{\partial w}{\partial y} = v \frac{\partial^2 w}{\partial y^2} - 2\Omega u - \frac{v}{K} w - \frac{\sigma_0 B_0^2 u w}{\rho x} \quad (3)$$

$$u \frac{\partial T}{\partial x} + v \frac{\partial T}{\partial y} = \frac{1}{\rho C_p} \frac{\partial}{\partial y} \left[k(T) \frac{\partial T}{\partial y} \right] + \frac{Q_0 (T - T_\infty)}{\rho C_p} - \frac{\alpha}{k_\infty} \left(\frac{\partial q_r}{\partial y} \right) + \frac{v}{C_p} \left(\frac{\partial u}{\partial y} \right)^2 \quad (4)$$

$$u \frac{\partial C}{\partial x} + v \frac{\partial C}{\partial y} = D_m \frac{\partial^2 C}{\partial y^2} - k_0 (C - C_\infty)^n \quad (5)$$

and the boundary condition for the model is

$$\left. \begin{aligned} u = U, v = 0, w = 0, T = T_w, C = C_w \text{ at } y = 0 \\ u \rightarrow 0, w \rightarrow 0, T \rightarrow T_\infty, C \rightarrow C_\infty \text{ as } y \rightarrow \infty \end{aligned} \right\} \quad (6)$$

where, U is the uniform velocity, β is the inclination angle of the plate with x -axis, C_p is the specific heat at constant pressure, $k(T)$ is the temperature dependent thermal conductivity, Q_0 is the heat source, D_m is the mass diffusivity, k_0 is the reaction rate, $k_0 > 0$ for destructive reaction, $k_0 = 0$ for no reaction and $k_0 < 0$ for generative reaction, n (integer) is the order of chemical reaction, T_w and C_w is the temperature and concentration respectively at wall and T_∞ and C_∞ is the temperature and concentration respectively far away from the plate.

175

176 2.1 METHOD OF SOLUTION

177

178 Introducing the following dimensionless variables;

$$x' = \frac{xU}{v}, y' = \frac{yU}{v}, u' = \frac{u}{U}, v' = \frac{v}{U}, w' = \frac{w}{U}, \theta = \frac{T - T_\infty}{T_w - T_\infty} \text{ and } \phi = \frac{C - C_\infty}{C_w - C_\infty}$$

180 ~~From the above dimensionless variables,~~ the following equations are obtained,

$$u = U u', v = U v', w = U w', T = T_\infty + (T_w - T_\infty) \theta \text{ and } C = C_\infty + (C_w - C_\infty) \phi \quad \text{to} \quad (7)$$

182 Now, by using equations (7), the equations (1), (2), (3), (4) and (5) are transformed as

$$\frac{\partial u'}{\partial x'} + \frac{\partial v'}{\partial y'} = 0 \quad (8)$$

$$u' \frac{\partial u'}{\partial x'} + v' \frac{\partial u'}{\partial y'} = \frac{\partial^2 u'}{\partial y'^2} + 2R' w' - \gamma u' - \frac{M u'^2}{x'} + G_r \theta \cos \beta + G_m \phi \cos \beta \quad (9)$$

$$u' \frac{\partial w'}{\partial x'} + v' \frac{\partial w'}{\partial y'} = \frac{\partial^2 w'}{\partial y'^2} - 2R' u' - \gamma w' - \frac{M u' w'}{x'} \quad (10)$$

$$u' \frac{\partial \theta}{\partial x'} + v' \frac{\partial \theta}{\partial y'} - \frac{1}{Pr} \left[(1 + T_c \theta + R) \frac{\partial^2 \theta}{\partial y'^2} + T_c \left(\frac{\partial \theta}{\partial y'} \right)^2 \right] - Q\theta - E_c \left(\frac{\partial u}{\partial y} \right)^2 = 0 \quad (11)$$

$$u' \frac{\partial \phi}{\partial x'} + v' \frac{\partial \phi}{\partial y'} - \frac{1}{Sc} \frac{\partial^2 \phi}{\partial y'^2} + \lambda \phi^n = 0 \quad (12)$$

187 ~~Now, using the equations (7), in the boundary condition (6) yield to,~~ becomes

$$\left. \begin{aligned} u' = 1, v' = 0, w' = 0, \theta = 1, \phi = 1 \text{ at } y' = 0 \\ u' \rightarrow 0, w' \rightarrow 0, \theta \rightarrow 0, \phi \rightarrow 0 \text{ as } y' \rightarrow \infty \end{aligned} \right\} \quad (13)$$

190 where,

$$191 \quad R' = \frac{\Omega v}{U^2}, \gamma = \frac{v^2}{KU^2}, M = \frac{\sigma_0 B_0^2}{\rho}, G_r = \frac{g \beta_r (T_w - T_\infty) v}{U^3}, G_m = \frac{g \beta_c (C_w - C_\infty) v}{U^3}, T_c = c(T_w - T_\infty),$$

$$192 \quad R = \frac{16 \sigma_s T_\infty^3}{3 \kappa^* k_\infty}, P_r = \frac{v}{\alpha}, Q = \frac{Q_0 v}{\rho C_p U^2}, E_c = \frac{U^2}{C_p (T_w - T_\infty)}, S_c = \frac{v}{D_m} \text{ and } \lambda = \frac{k_0 (C_w - C_\infty)^{n-1} v}{U^2}$$

193 In order to deal with the problem, introducing the potential ψ (since the flow is
194 incompressible) is defined by

$$195 \quad u' = \frac{\partial \psi}{\partial y'}, v' = -\frac{\partial \psi}{\partial x'} \quad (14)$$

196 The mathematical significance of using the equation (14) is that the continuity equation (8) is
197 satisfied automatically.

198 Now, with the help of equation (14), the equations (9), (10), (11) and (12) respectively
199 transformed as follows,

$$200 \quad \frac{\partial \psi}{\partial y'} \frac{\partial^2 \psi}{\partial x' \partial y'} - \frac{\partial \psi}{\partial x'} \frac{\partial^2 \psi}{\partial y'^2} - \frac{\partial^3 \psi}{\partial y'^3} - 2R' w' + \gamma \frac{\partial \psi}{\partial y'} + \frac{M}{x'} \left(\frac{\partial \psi}{\partial y'} \right)^2 - G_r \theta \cos \beta - G_m \phi \cos \beta = 0 \quad (15)$$

$$201 \quad \frac{\partial \psi}{\partial y'} \frac{\partial w'}{\partial x'} - \frac{\partial \psi}{\partial x'} \frac{\partial w'}{\partial y'} - \frac{\partial^2 w'}{\partial y'^2} + 2R' \frac{\partial \psi}{\partial y'} + \gamma w' + \frac{M}{x'} \frac{\partial \psi}{\partial y'} w' = 0 \quad (16)$$

$$202 \quad \frac{\partial \psi}{\partial y'} \frac{\partial \theta}{\partial x'} - \frac{\partial \psi}{\partial x'} \frac{\partial \theta}{\partial y'} - \frac{1}{P_r} \left[(1 + T_c \theta + R) \frac{\partial^2 \theta}{\partial y'^2} + T_c \left(\frac{\partial \theta}{\partial y'} \right)^2 \right] - Q \theta - E_c \left(\frac{\partial^2 \psi}{\partial y'^2} \right)^2 = 0 \quad (17)$$

$$203 \quad \frac{\partial \psi}{\partial y'} \frac{\partial \phi}{\partial x'} - \frac{\partial \psi}{\partial x'} \frac{\partial \phi}{\partial y'} - \frac{1}{S_c} \frac{\partial^2 \phi}{\partial y'^2} + \lambda \phi^n = 0 \quad (18)$$

204 and the boundary conditions (13) become,

$$205 \quad \left. \begin{aligned} \frac{\partial \psi}{\partial y'} = 1, \frac{\partial \psi}{\partial x'} = 0, w' = 0, \theta = 1, \phi = 1 \text{ at } y' = 0 \\ \frac{\partial \psi}{\partial y'} \rightarrow 0, w' \rightarrow 0, \theta \rightarrow 0, \phi \rightarrow 0 \text{ as } y' \rightarrow \infty \end{aligned} \right\} \quad (19)$$

206 Finding the similarity solution of the equations (15) to (18) is equivalent to determining the
207 invariant solutions of these equations under a particular continuous one parameter group.
208 Introducing the simplified form of Lie-group transformations [8] namely, the scaling group of
209 transformations

$$210 \quad G_1: x^* = x' e^{\varepsilon \alpha_1}, y^* = y' e^{\varepsilon \alpha_2}, \psi^* = \psi e^{\varepsilon \alpha_3}, w^* = w' e^{\varepsilon \alpha_4}, \theta^* = \theta e^{\varepsilon \alpha_5} \text{ and } \phi^* = \phi e^{\varepsilon \alpha_6} \quad (20)$$

211 Here, $\varepsilon (\neq 0)$ is the parameter of the group and α 's are arbitrary real numbers whose
212 interrelationship will be determined by our analysis. Equations (20) may be considered as a
213 point transformation which transforms the coordinates $(x', y', \psi, w', \theta, \phi)$ to the coordinates

$$214 \quad (x^*, y^*, \psi^*, w^*, \theta^*, \phi^*).$$

215 The system will remain invariant under the group transformation G_1 , so the following
216 relations among the exponents are obtained from equations (15) to (18),

$$\left. \begin{aligned} \alpha_1 + 2\alpha_2 - 2\alpha_3 &= 3\alpha_2 - \alpha_3 = -\alpha_4 = \alpha_2 - \alpha_3 = -\alpha_5 = -\alpha_6 \\ \alpha_1 + \alpha_2 - \alpha_3 - \alpha_4 &= 2\alpha_2 - \alpha_4 = \alpha_2 - \alpha_3 = -\alpha_4 \\ \alpha_1 + \alpha_2 - \alpha_3 - \alpha_5 &= 2\alpha_2 - \alpha_5 = 2\alpha_2 - 2\alpha_5 = 4\alpha_2 - 2\alpha_3 \\ \alpha_1 + \alpha_2 - \alpha_3 - \alpha_6 &= 2\alpha_2 - \alpha_6 = -n\alpha_6 \end{aligned} \right\} \quad (21)$$

Again, the following relations are obtained from the boundary conditions (19),

$$\begin{aligned} \alpha_2 &= \alpha_3 \\ \alpha_5 &= \alpha_6 = 0 \end{aligned} \quad (22)$$

Solving the system of linear equations (21) and (22), the following relationship are obtained,

$$\alpha_1 = 2\alpha_2 = 2\alpha_3, \alpha_4 = \alpha_5 = \alpha_6 = 0$$

By using the above relation, the equation (20) i.e. G_+ reduces to the following one-parameter group of transformations

$$x^* = x'e^{2\epsilon\alpha_2}, y^* = y'e^{\epsilon\alpha_2}, \psi^* = \psi e^{\epsilon\alpha_2}, w^* = w', \theta^* = \theta, \varphi^* = \varphi \quad (23)$$

Expanding by Taylor's method in powers of ϵ and keeping terms up to the order ϵ , then from equation (23) is obtained as we have

$$x^* - x' = 2\epsilon x' \alpha_2, y^* - y' = \epsilon y' \alpha_2, \psi^* - \psi = \epsilon \psi \alpha_2, w^* - w' = 0, \theta^* - \theta = 0, \varphi^* - \varphi = 0$$

In terms of differential these yield to

$$\frac{dx'}{2\alpha_2 x'} = \frac{dy'}{\alpha_2 y'} = \frac{d\psi}{\alpha_2 \psi} = \frac{dw'}{0} = \frac{d\theta}{0} = \frac{d\varphi}{0} \quad (24)$$

Solving the equation (24) the following equations are obtained,

$$\eta = \frac{y'}{\sqrt{x'}}, \psi = \sqrt{x'} f(\eta), w' = g_0(\eta), \theta = \theta(\eta) \text{ and } \varphi = \varphi(\eta)$$

By using the above mentioned variables, the equations (15), (16), (17) and (18) have been obtained respectively as becomes

$$f''' + \frac{1}{2} f f'' - M f'^2 + 2R' g_0 - \gamma f' + G_r \theta \cos \beta + G_m \varphi \cos \beta = 0 \quad (25)$$

$$g_0'' + \frac{1}{2} f g_0' - 2R' f' - \gamma g_0 - M f' g_0 = 0 \quad (26)$$

$$\frac{1}{P_r} (1 + T_c \theta + R) \theta'' + \frac{1}{P_r} T_c \theta'^2 + \frac{1}{2} f \theta' + Q \theta + E_c f''^2 = 0 \quad (27)$$

$$\frac{1}{S_c} \varphi'' + \frac{1}{2} f \varphi' - \lambda \varphi^n = 0 \quad (28)$$

The corresponding boundary conditions (19) become

$$\left. \begin{aligned} f' = 1, f = 0, g_0 = 0, \theta = 1, \varphi = 1 \text{ at } \eta = 0 \\ f' \rightarrow 0, g_0 \rightarrow 0, \theta \rightarrow 0, \varphi \rightarrow 0 \text{ as } \eta \rightarrow \infty \end{aligned} \right\} \quad (29)$$

In the previous equations (25) to (29), primes denote differentiation with respect to η only and the parameters are defined as

$$M = \frac{\sigma_0 B_0^2}{\rho} \text{ is the magnetic parameter}$$

243 $\gamma = \frac{v^2 x'}{KU^2}$ is the porosity parameter

244 $R' = \frac{\Omega v x'}{U^2}$ is the rotational parameter

245 $G_r = \frac{g \beta_T (T_w - T_\infty) v x'}{U^3}$ is the Grashof number

246 $G_m = \frac{g \beta_c (C_w - C_\infty) v x'}{U^3}$ is the modified Grashof number

247 $T_c = c(T_w - T_\infty)$ is the thermal conductivity parameter

248 $P_r = \frac{v}{\alpha}$ is the Prandtl number

249 $R = \frac{16\sigma_s T_\infty^3}{3\kappa^* k_\infty}$ is the radiation parameter

250 $Q = \frac{Q_0 v}{\rho C_p U^2}$ is the heat source parameter

251 $E_c = \frac{U^2}{C_p (T_w - T_\infty)}$ is Eckert number

252 $S_c = \frac{v}{D_m}$ is the Schmidt number

253 $\lambda = \frac{k_0 (C_w - C_\infty)^{n-1} v}{U^2}$ is the reaction parameter

254 and n (integer) is the order of chemical reaction

255

256 **2.2 SKIN-FRICTION COEFFICIENTS, NUSSELT AND SHERWOOD NUMBER**

257

258 The physical quantities of the skin-friction coefficient, the reduced Nusselt number and
259 reduced Sherwood number are calculated respectively by the following equations,

260 $C_f (R_e)^{\frac{1}{2}} = -f''(0)$ (30)

261 $C_{g_0} (R_e)^{\frac{1}{2}} = -g'_0(0)$ (31)

262 $N_u (R_e)^{-\frac{1}{2}} = -\theta'(0)$ (32)

263 $S_h (R_e)^{-\frac{1}{2}} = -\phi'(0)$ (33)

264 where, $R_e = \frac{U x'}{v}$ is the Reynolds number.

265

3. RESULTS AND DISCUSSION

The heat and mass transfer problem associated with laminar flow past an inclined plate of a rotating system has been studied. In order to investigate the physical representation of the problem, the numerical values of primary velocity, secondary velocity, temperature and species concentration from equations (25), (26), (27) and (28) with the boundary layer have been computed for different parameters as the magnetic parameter (M), the rotational parameter (R'), the porosity parameter (γ), the Grashof number (G_r), the modified Grashof number (G_m), the radiation parameter (R), the Prandtl number (Pr), the Eckert number (Ec), the thermal conductivity parameter (T_c), the heat source parameter (Q), the Schmidt number (Sc), the reaction parameter (λ), the inclination angle (β) and the order of chemical reaction (n) respectively.

Figs. 2a and 2b show typical profiles for primary velocity (f') and secondary velocity (g_0) for different values of magnetic parameter, respectively. It is observed that as the magnetic parameter increased, the primary and secondary velocities are decreased and increased respectively, where other parameters have the value $R' = Gr = Gm = \gamma = Pr = Tc = R = 0.1$,

$$Q = Ec = Sc = \lambda = 0.1, \beta = 60^\circ, n = 1$$

Figs. 3a, 3b, 3c and 3d present typical profiles for primary velocity (f'), secondary velocity (g_0), temperature (θ) and concentration (ϕ) for different values of rotational parameter, respectively. It is observed that as the rotational parameter increased, the primary velocity is decreased where as the secondary velocity, temperature and concentration is increased respectively, where other parameters have the value

$$M = Gr = Gm = \gamma = Pr = Tc = R = Q = Ec = Sc = 0.1, \lambda = 0.1, \beta = 60^\circ, n = 1$$

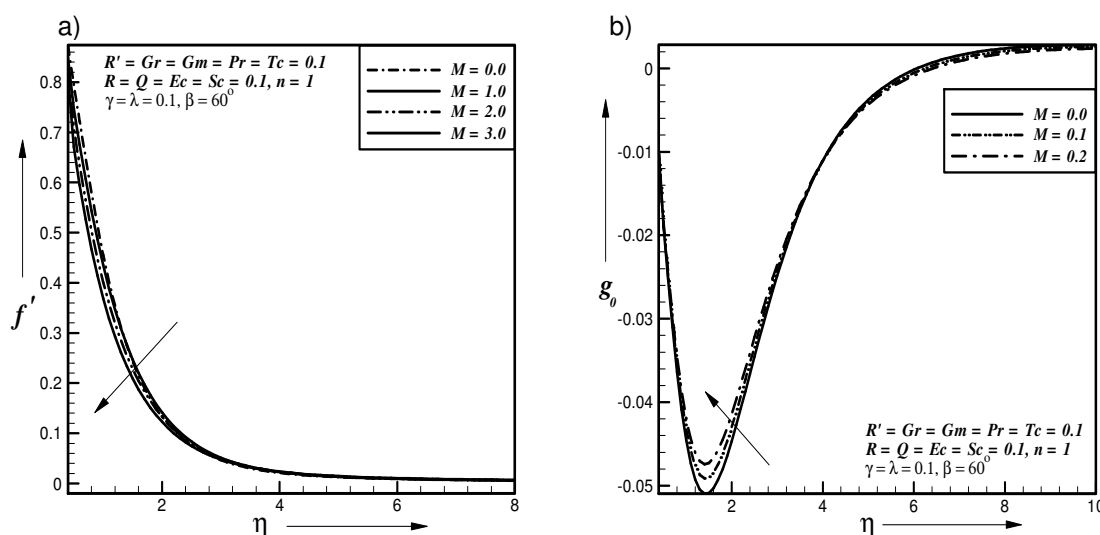
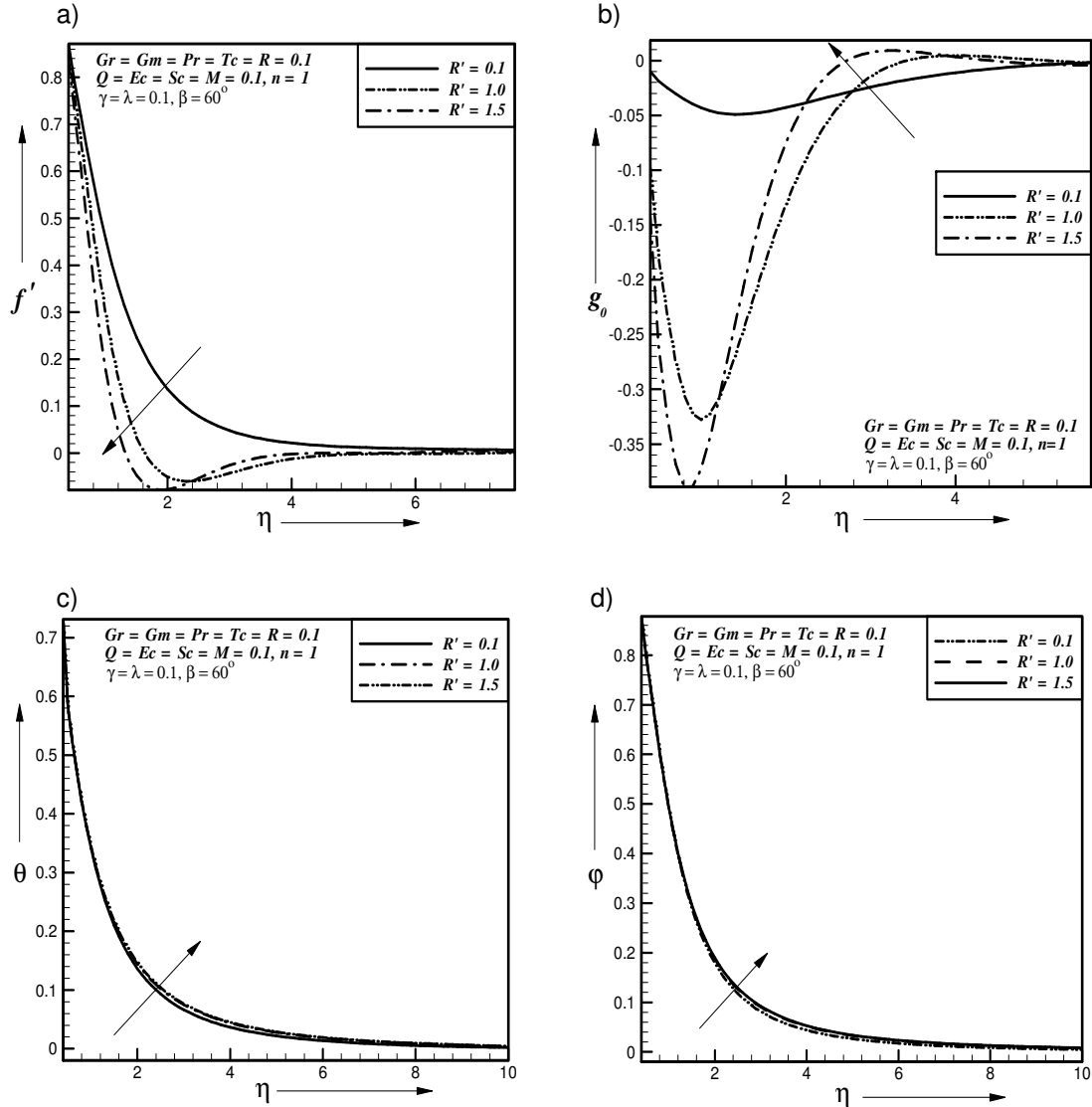


Fig. 2. Effect of magnetic parameter on a) primary velocity b) secondary velocity profiles

297



298

299

300

301

302

303

304

305

306

307

308

309

310

311

312

313

314

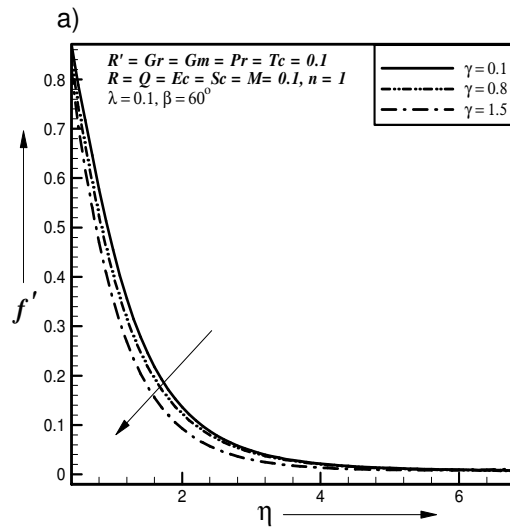
315

316

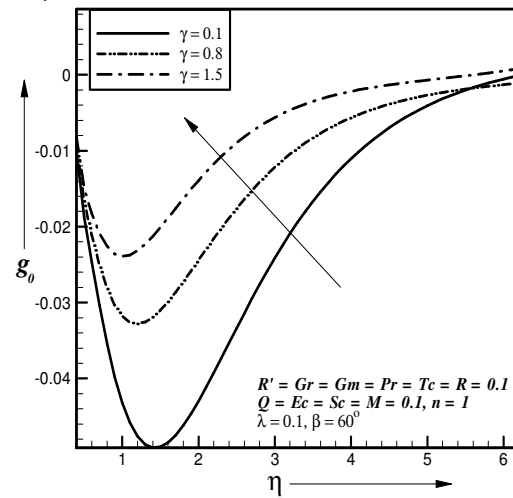
Fig. 3. Effect of rotational parameter on a) primary velocity b) secondary velocity c) temperature d) concentration profiles

Figs. 4a, 4b, 4c and 4d show typical profiles for primary velocity (f'), secondary velocity (g_0), temperature (θ) and concentration (ϕ) for different values of porosity parameter γ , respectively. It is observed that as the porosity parameter increased, the primary velocity is decreased where as the secondary velocity, temperature and concentration is increased respectively, where other parameters have the value $M = R' = Gr = Gm = Pr = Tc = R = Q = Ec = Sc = \lambda = 0.1, \beta = 60^\circ, n = 1$.

317



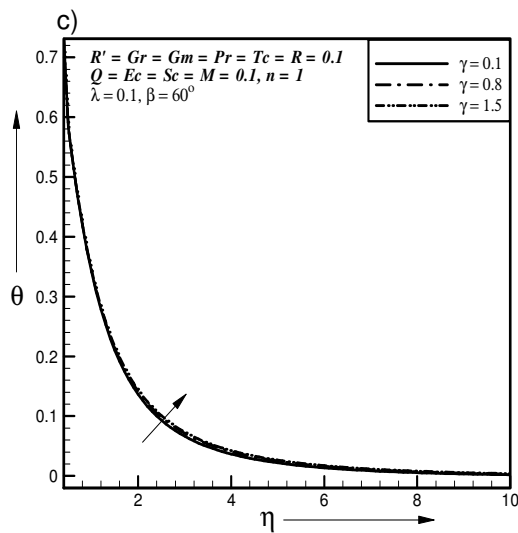
b)



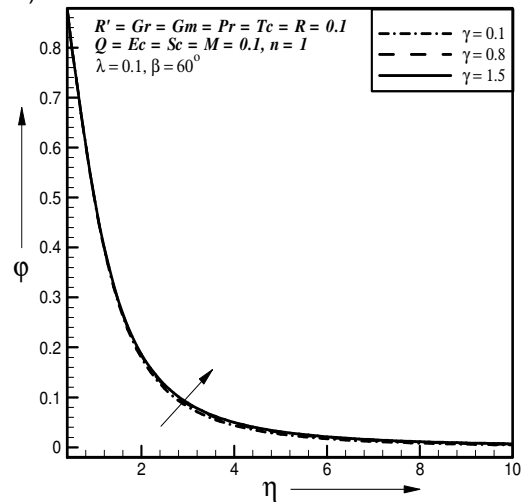
318

319

320



d)



321

322

323

324

325

Fig. 4. Effect of porosity parameter on a) primary velocity b) secondary velocity c) temperature d) concentration profiles

326

Figs. 5a and 5b present typical profiles for primary velocity (f') and secondary

327

velocity (g_0) for different values of inclination angle, respectively. It is observed that as the

328

inclination angle increased, the primary and secondary velocities are decreased and

329

increased respectively, where other parameters have the value $M = R' = Gr = Gm = \gamma = 0.1$,

330

$Pr = Tc = R = Q = Ec = Sc = \lambda = 0.1, n = 1$.

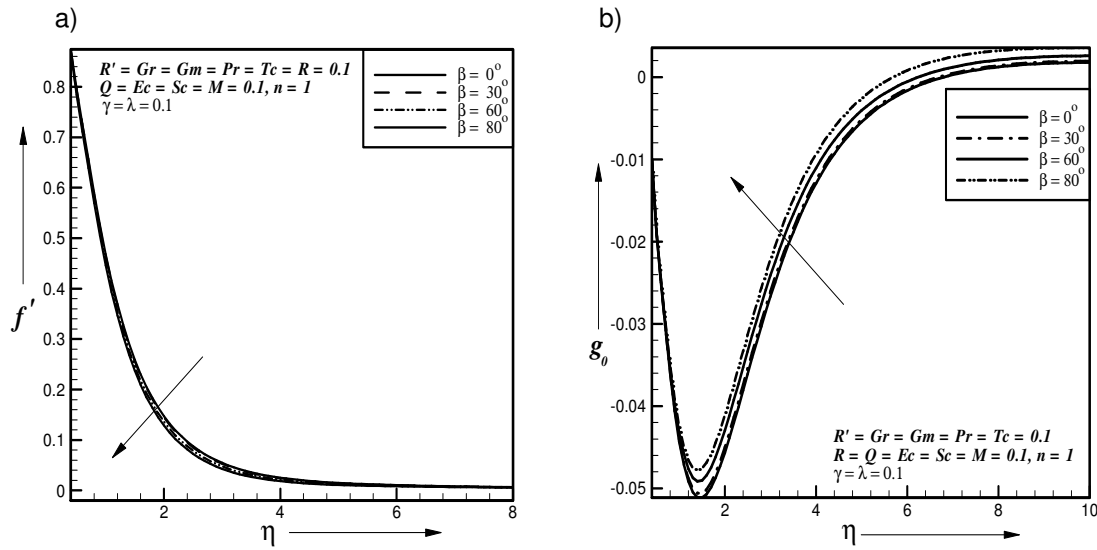
331

332

333

334

335



336

337

338

339

Fig. 5. Effect of inclination angle on a) primary velocity b) secondary velocity profiles

340

341

342

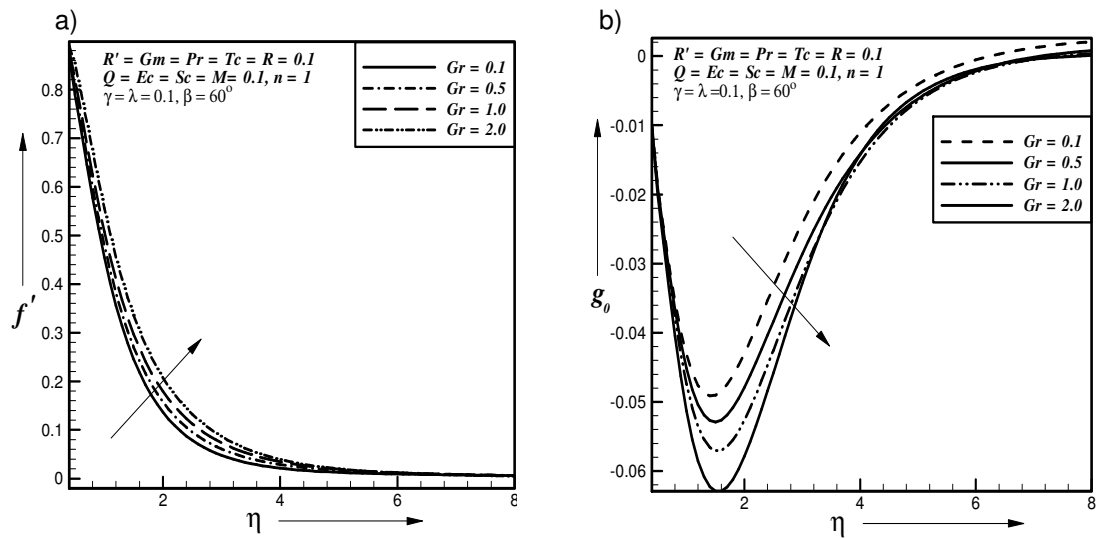
343

344

345

346

Figs. 6a, 6b and 6c present typical profiles for primary velocity (f'), secondary velocity (g_θ) and temperature (θ) for different values of Grashof number, respectively. It is observed that as the Grashof number increased, the primary velocity is increased where as the secondary velocity and temperature is decreased respectively, where other parameters have the value $M = R' = \gamma = Gm = Pr = Tc = R = Q = Ec = Sc = \lambda = 0.1$, $\beta = 60^\circ$, $n = 1$.



347

348

349

350

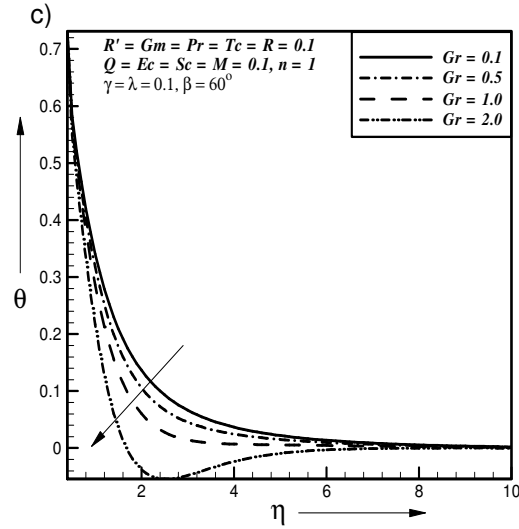
351

352

353

354

355



356

357

358

359

360

Fig. 6. Effect of Grashof number on a) primary velocity b) secondary velocity c) temperature profiles

361

362

363

364

365

366

367

368

369

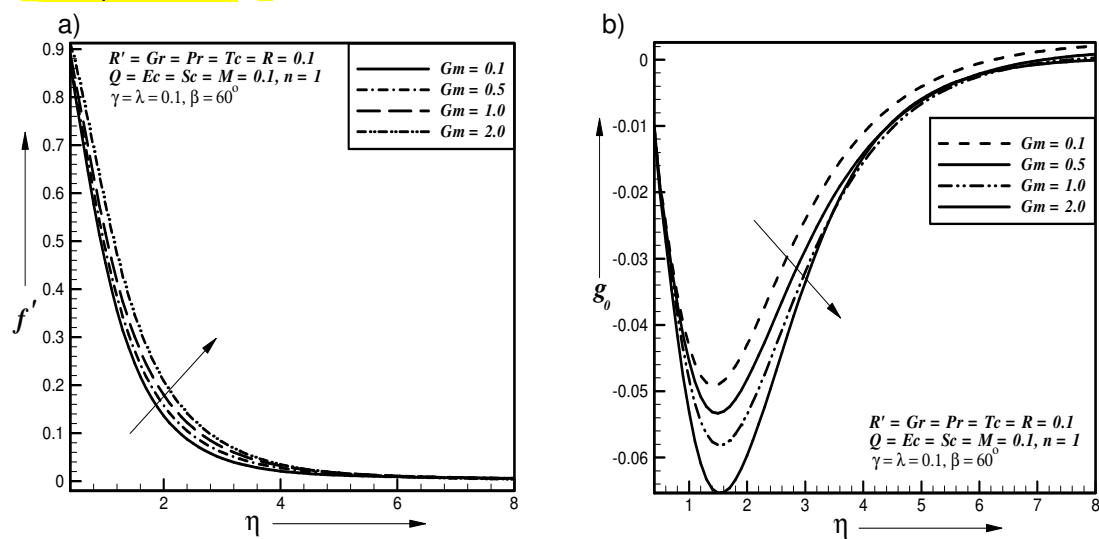
370

371

372

Figs. 7a, 7b and 7c show typical profiles for primary velocity (f'), secondary velocity (g_0) and concentration (ϕ) for different values of modified Grashof number, respectively. It is observed that as the modified Grashof number increased, the primary velocity is increased where as the secondary velocity and concentration is decreased respectively, where other parameters have the value $M = R' = \gamma = Gr = Pr = Tc = R = Q = Ec = Sc = \lambda = 0.1$, $\beta = 60^\circ$, $n = 1$.

Figs. 8a and 8b present typical profiles for primary velocity (f') and temperature (θ) for different values of Prandtl number, respectively. It is observed that as the Prandtl number increased, the primary velocity and temperature is increased and decreased respectively, where other parameters have the value $M = R' = Gr = Gm = \gamma = Tc = R = Q = Ec = Sc = 0.1$, $\lambda = 0.1$, $\beta = 60^\circ$, $n = 1$.



373

374

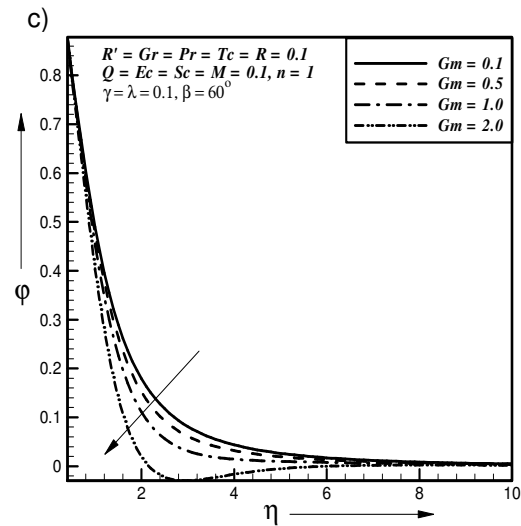


Fig. 7. Effect of modified Grashof number on a) primary velocity b) secondary velocity c) concentration profiles

375
376
377
378
379
380

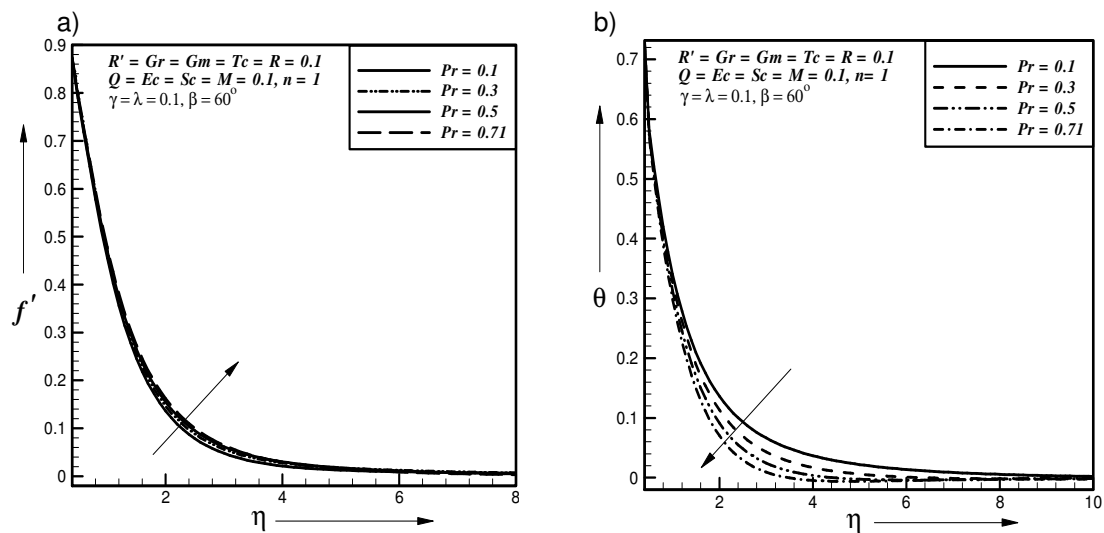


Fig. 8. Effect of Prandtl number on a) primary velocity b) temperature profiles

381
382
383
384

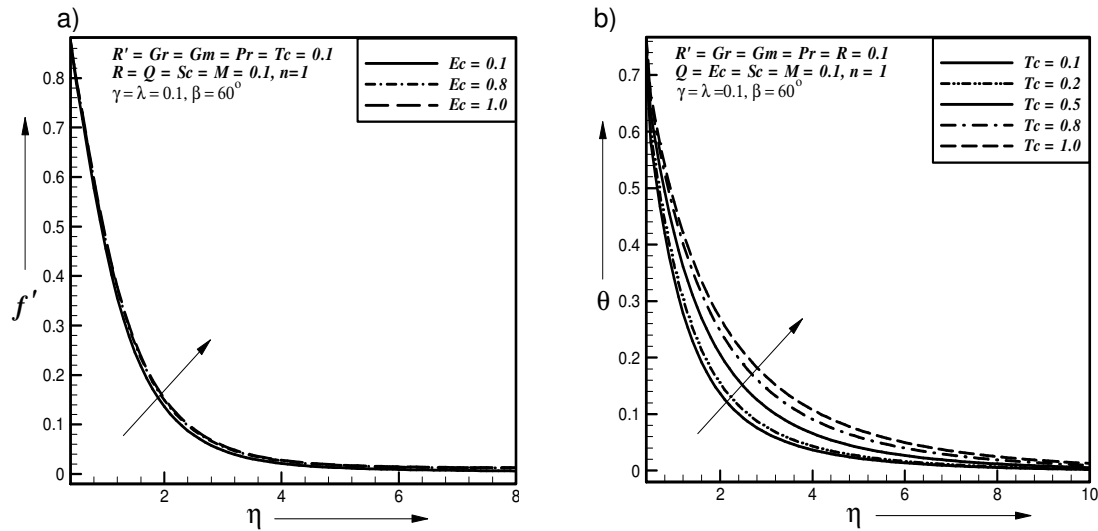
Fig. 9a displays typical profiles for primary velocity (f') for different values of Eckert number. It is observed that the primary velocity is increased with the increase of Eckert number, where other parameters have the value $M = Gr = Gm = \gamma = Pr = Tc = R = Q = R' = Sc = 0.1$, $\lambda = 0.1, \beta = 60^\circ, n = 1$.

388

Fig. 9b displays typical profiles for temperature (θ) for different values of Thermal conductivity parameter. It is observed that the temperature is increased with the increase of Thermal conductivity parameter, where other parameters have the value $M = Gr = Gm = \gamma = Pr = 0.1$, $Ec = R = Q = R' = Sc = \lambda = 0.1, \beta = 60^\circ, n = 1$.

392
393
394

395



396

397

398

399

Fig. 9. Effect of a) Eckert number on primary velocity profiles b) thermal conductivity parameter on temperature profiles

400

Fig. 10a represents typical profiles for concentration (ϕ) for different values of Schmidt

401

number Sc . It is observed that the concentration is decreased with the increase of Schmidt

402

number, where other parameters have the value $M = Gr = Gm = \gamma = Pr = Ec = Q = 0.1$,

403

$Tc = R' = R = \lambda = 0.1$, $\beta = 60^\circ$, $n = 1$.

404

Fig. 10b represents typical profiles for concentration (ϕ) for different values of reaction

405

parameter λ . The no reaction ($\lambda = 0.0$) and destructive reaction ($\lambda > 0.0$) is studied. It is

406

observed that the concentration is decreased with the increase of reaction parameter, where

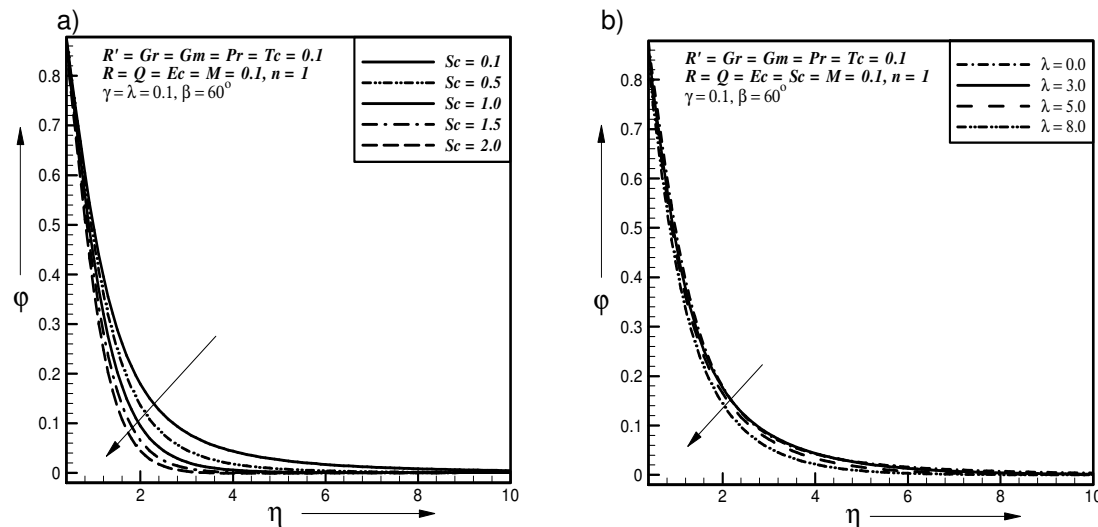
407

other parameters have the value $M = Gr = Gm = \gamma = Pr = Ec = Q = Tc = R' = R = Sc = 0.1$,

408

$\beta = 60^\circ$, $n = 1$.

409



410

411

412

413

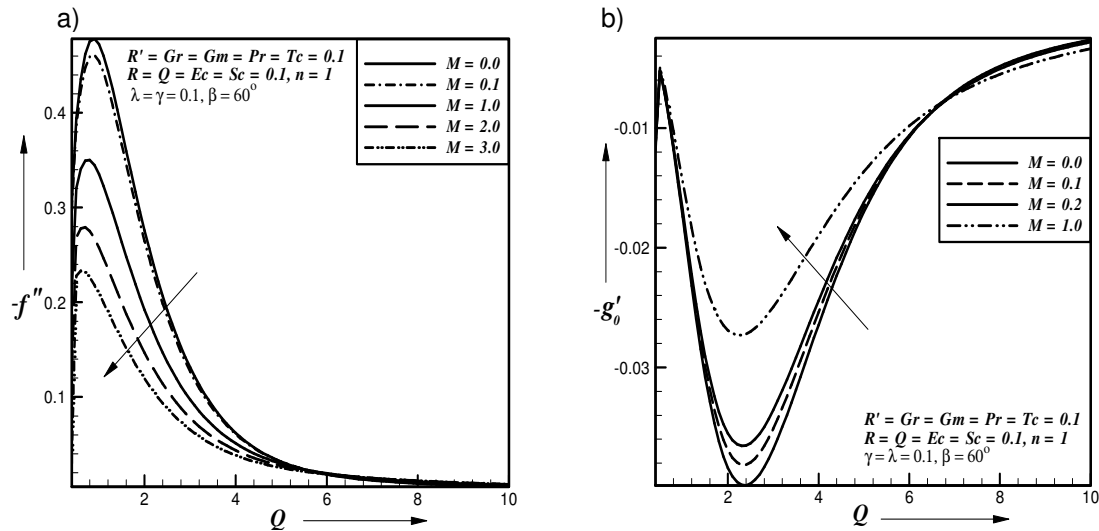
Fig. 10. Effect of a) Schmidt number on concentration profiles b) reaction parameter on concentration profiles

For the physical interest of the problem, the dimensionless skin-friction coefficient $(-f'')$ and $(-g'_0)$, the dimensionless heat transfer rate $(-\theta')$ at the plate and the dimensionless mass transfer rate $(-\phi')$ at the plate are plotted against Heat source parameter (Q) and illustrated in Figs. 11-19.

Figs. 11a and 11b represent the primary shear stress $(-f'')$ and secondary shear stress $(-g'_0)$ which are plotted against heat source parameter (Q) for different values of magnetic parameter. It is observed that the primary shear stress is decreased and secondary shear stress is increased with the increase of magnetic parameter, where other parameters have the value $R' = Gr = Gm = \gamma = Pr = Ec = Q = Tc = R = Sc = \lambda = 0.1, \beta = 60^\circ, n = 1$.

Figs. 12a and 12b represent the primary shear stress $(-f'')$ and secondary shear stress $(-g'_0)$ which are plotted against heat source parameter (Q) for different values of rotational parameter. It is observed that the primary shear stress is decreased and secondary shear stress is increased with the increase of rotational parameter, where other parameters have the value $M = Gr = Gm = \gamma = Pr = Ec = Q = Tc = R = Sc = \lambda = 0.1, \beta = 60^\circ, n = 1$.

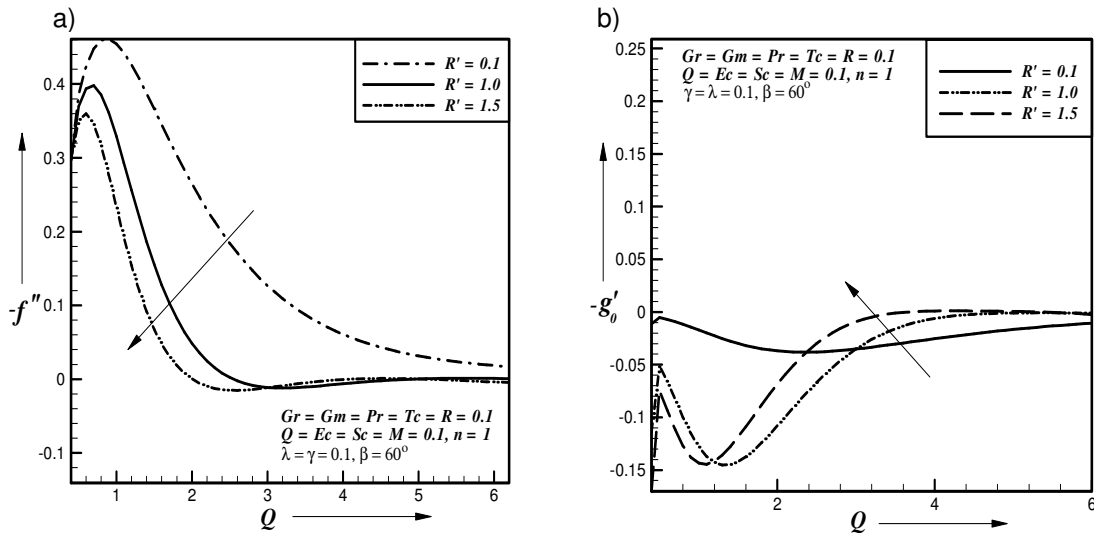
428
429



430
431
432
433
434
435
436
437
438
439
440
441
442
443
444
445
446

Fig. 11. Effect of magnetic parameter on a) primary shear stress b) secondary shear stress

447



448

449

450

451

Fig. 12. Effect of rotational parameter on a) primary shear stress b) secondary shear stress

452

453

454

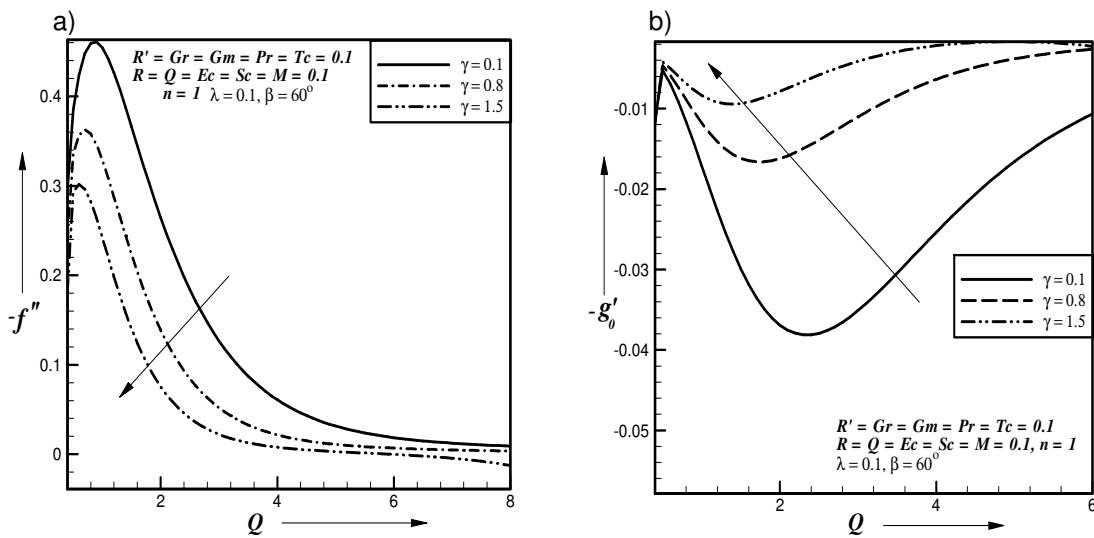
455

456

457

458

Figs. 13a and 13b represent the primary shear stress $(-f'')$ and secondary shear stress $(-g'_0)$ which are plotted against heat source parameter (Q) for different values of porosity parameter. It is observed that the primary shear stress is decreased and secondary shear stress is increased with the increase of porosity parameter, where other parameters have the value $M = Gr = Gm = R' = Pr = Ec = Q = Tc = R = Sc = \lambda = 0.1, \beta = 60^\circ, n = 1$.



459

460

461

462

Fig. 13. Effect of porosity parameter on a) primary b) secondary shear stress

463

464

Fig. 14a represents the primary shear stress $(-f'')$ which is plotted against heat source parameter (Q) for different values of Grashof number. It is observed that the primary shear

stress is increased with the increase of Grashof number, where other parameters have the value $M = \gamma = Gm = R' = Pr = Ec = Q = Tc = R = Sc = \lambda = 0.1, \beta = 60^\circ, n = 1$.

Fig. 14b represents the primary shear stress $(-f'')$ which is plotted against heat source parameter (Q) for different values of modified Grashof number. It is observed that the primary shear stress is increased with the increase of modified Grashof number, where other parameters have the value $M = \gamma = Gr = R' = Pr = Ec = Q = Tc = R = Sc = \lambda = 0.1, \beta = 60^\circ, n = 1$.

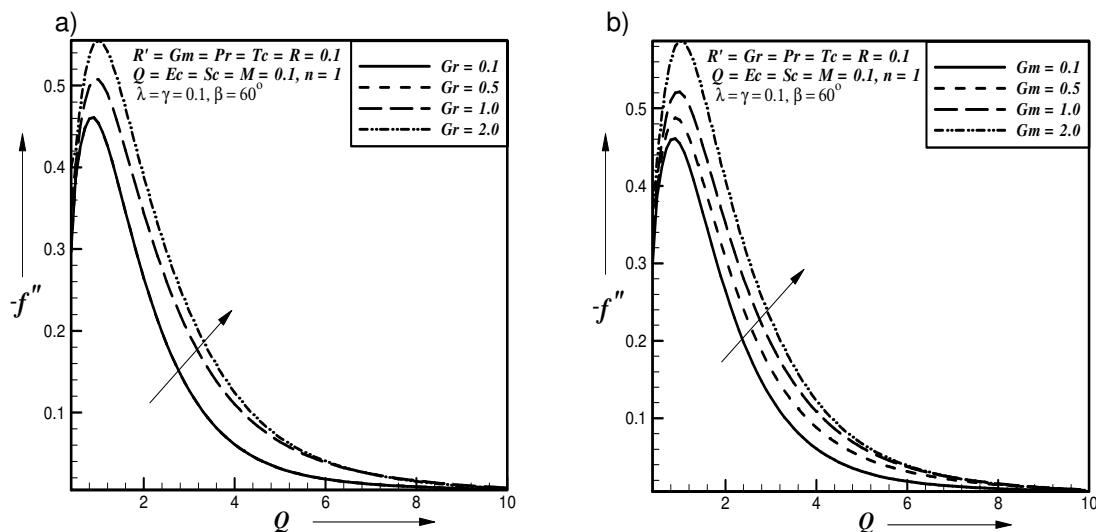


Fig. 14. Effect of a) Grashof number b) modified Grashof on primary shear stress

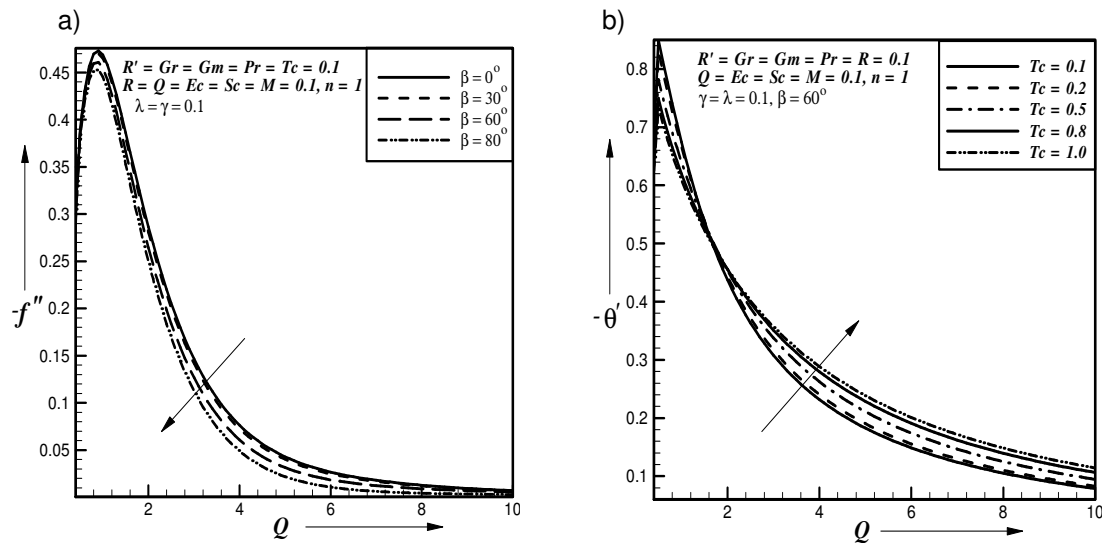
Fig. 15a represents the primary shear stress $(-f'')$ which is plotted against heat source parameter (Q) for different values of inclination angle. It is observed that the primary shear stress is decreased with the increase of inclination angle, where other parameters have the value $M = \gamma = Gm = Gr = R' = Pr = Ec = Q = Tc = R = Sc = \lambda = 0.1, n = 1$.

Fig. 15b represents the dimensionless heat transfer rate $(-\theta')$ which is plotted against Heat source parameter (Q) for different values of thermal conductivity parameter. It is observed that the heat transfer rate is increased with the increase of thermal conductivity parameter, where other parameters have the value $M = \gamma = Gm = Gr = R' = Pr = Ec = Q = R = Sc = 0.1, \lambda = 0.1, \beta = 60^\circ, n = 1$.

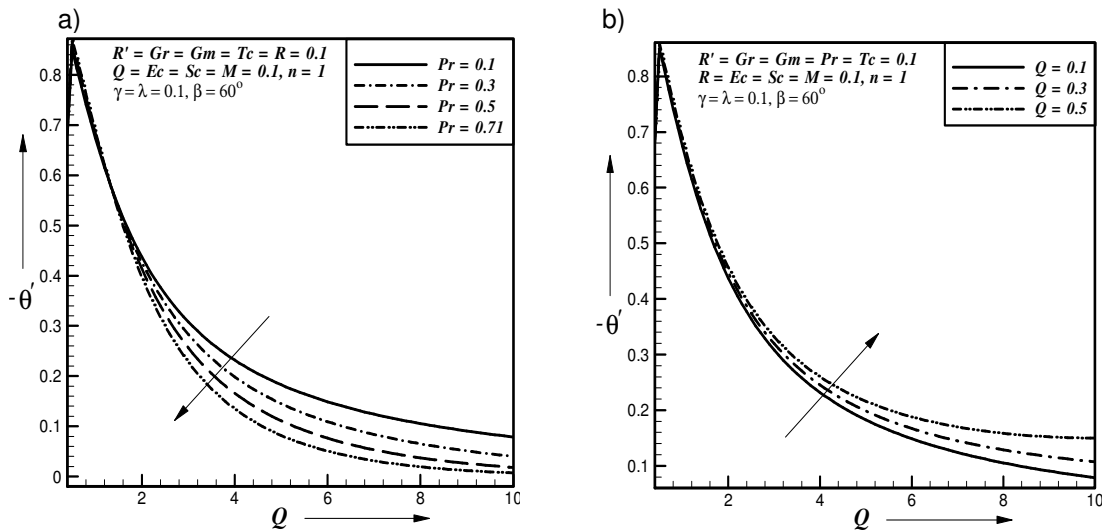
Fig. 16a represents the dimensionless heat transfer rate $(-\theta')$ which is plotted against heat source parameter (Q) for different values of Prandtl number. It is observed that the heat transfer rate is decreased with the increase of Prandtl number, where other parameters have the value $M = \gamma = Gm = Gr = R' = Tc = Ec = Q = R = Sc = \lambda = 0.1, \beta = 60^\circ, n = 1$.

Fig. 16b represents the dimensionless heat transfer rate $(-\theta')$ which is plotted against Heat source parameter (Q) for different values of heat source parameter. It is observed that the

493 heat transfer rate is increased with the increase of heat source parameter, where other
 494 parameters have the value $M = \gamma = Gm = Gr = R' = Tc = Ec = Pr = R = Sc = \lambda = 0.1, \beta = 60^\circ$,
 495 $n = 1$.
 496
 497



498
 499
 500 **Fig. 15. Effect of a) inclination angle on primary shear stress b) thermal conductivity**
 501 **parameter on heat transfer rate**
 502
 503



504
 505
 506 **Fig. 16. Effect of a) Prandtl number b) heat source parameter on heat transfer rate**
 507

508 Fig. 17a represents the dimensionless heat transfer rate $(-\theta')$ which is plotted against heat
 509 source parameter (Q) for different values of Eckert number. It is observed that the heat
 510 transfer rate is increased with the increase of Eckert number, where other parameters have
 511 the value $M = \gamma = Gm = Gr = R' = Tc = Q = Pr = R = Sc = \lambda = 0.1, \beta = 60^\circ, n = 1$.

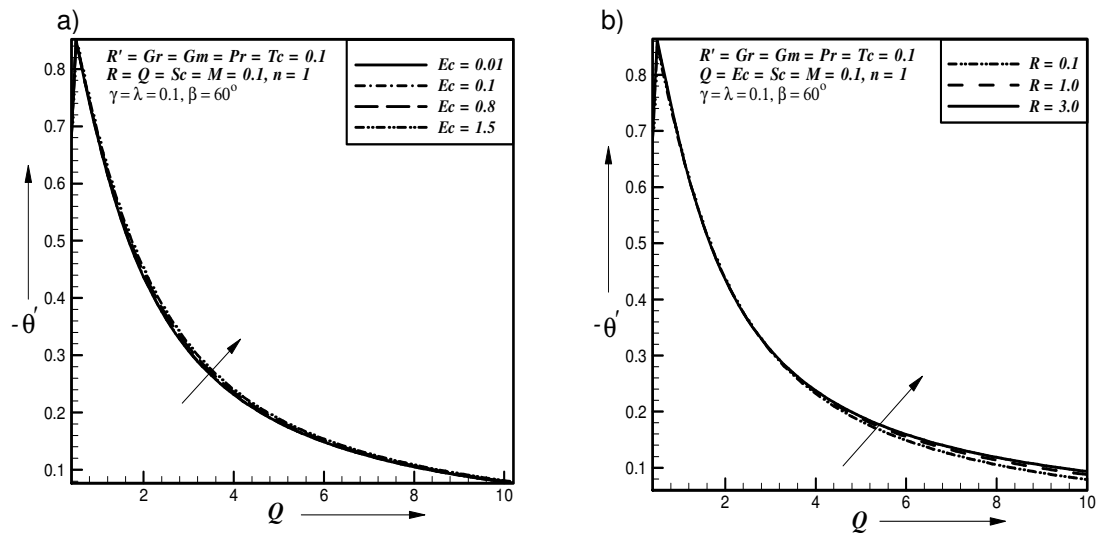
Fig. 17b represents the dimensionless heat transfer rate $(-\theta')$ which is plotted against heat source parameter (Q) for different values of radiation parameter. It is observed that the heat transfer rate is increased with the increase of radiation parameter, where other parameters have the value $M = \gamma = Gm = Gr = R' = Tc = Q = Pr = Ec = Sc = \lambda = 0.1$, $\beta = 60^\circ$, $n = 1$.

Fig. 18a represents the dimensionless mass transfer rate $(-\phi')$ which is plotted against heat source parameter (Q) for different values of Schmidt number. It is observed that the mass transfer rate is decreased with the increase of Schmidt number, where other parameters have the value $M = \gamma = Gm = Gr = R' = Tc = Q = Pr = Ec = R = \lambda = 0.1$, $\beta = 60^\circ$, $n = 1$.

Fig. 18b represents the dimensionless mass transfer rate $(-\phi')$ which is plotted against heat source parameter (Q) for different values of reaction parameter. It is observed that the mass transfer rate is decreased with the increase of reaction parameter, where other parameters have the value $M = \gamma = Gm = Gr = R' = Tc = Q = Pr = Ec = R = Sc = 0.1$, $\beta = 60^\circ$, $n = 1$.

Fig. 19 represents the dimensionless mass transfer rate $(-\phi')$ which is plotted against heat source parameter (Q) for different values of order of chemical reaction. It is observed that the mass transfer rate is increased with the increase of order of chemical reaction, where other parameters have the value $M = \gamma = Gm = Gr = R' = Tc = Q = Pr = Ec = \lambda = R = Sc = 0.1$, $\beta = 60^\circ$.

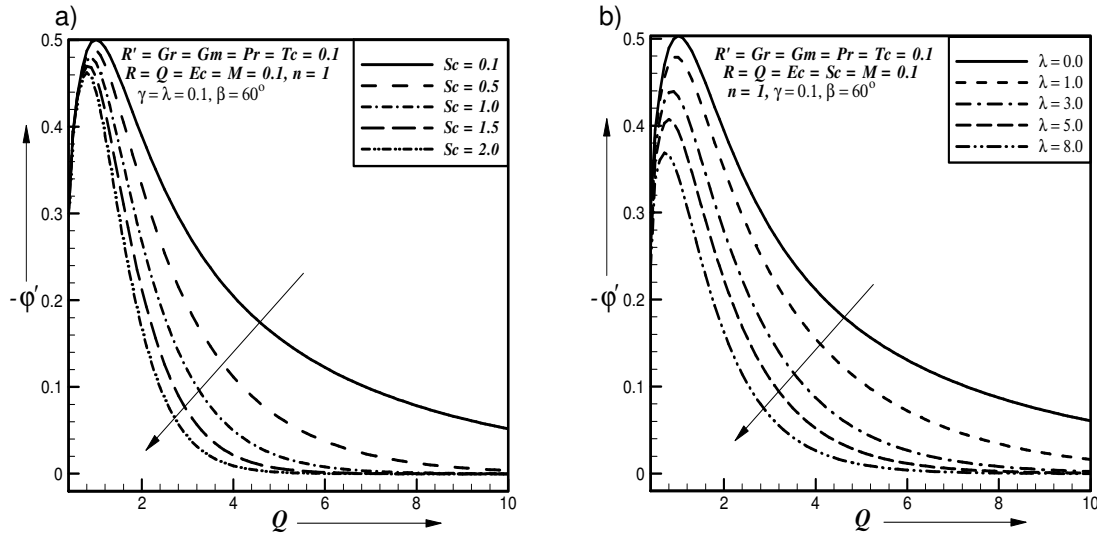
532
533



534
535
536
537
538
539
540
541
542

Fig. 17. Effect of a) Eckert number b) radiation parameter on heat transfer rate

543



544

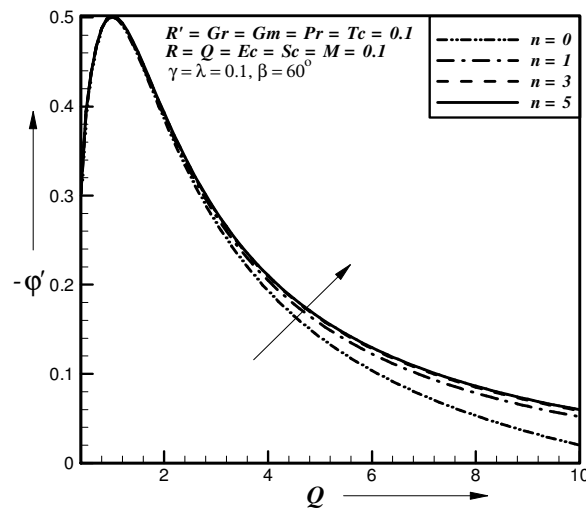
545

546

547

548

Fig. 18. Effect of a) Schmidt number b) reaction parameter on mass transfer rate



549

550

551

552

553

554

Fig. 19. Effect of order of chemical reaction on mass transfer rate

4. CONCLUSION

Laminar boundary layer flow past an inclined permeable plate of a rotating system with the influence of magnetic field, thermal radiation and chemical reaction has been investigated. The results are presented for various parameters. The velocity, temperature and concentration distributions for different parameters are shown graphically. The important findings of the investigation from graphical representation are listed below:

560

561

562

563

564

The primary velocity profiles are decreased due to increase of magnetic parameter where as the reverse effect is found for the secondary velocity profiles. Also the primary shear stress is decreased due to increase of magnetic parameter where as the reverse effect is found for secondary shear stress.

The primary velocity profiles and primary shear stress are decreased due to increase of rotational parameter where as the reverse effect is found for the secondary velocity profiles and secondary shear stress. Also the temperature and concentration boundary layer thickness are increased due to increase of rotational parameter.

The primary velocity profiles and primary shear stress are decreased due to increase of permeability of the porous medium where as the reverse effect is found for the secondary velocity profiles and secondary shear stress. Also the temperature and concentration boundary layer thickness are increased due to increase of permeability of the porous medium.

The primary velocity profiles and primary shear stress are decreased due to increase of inclination angle where as the reverse effect is found for the secondary velocity profiles.

The primary velocity profiles and primary shear stress are increased due to increase of Grashof number where as the reverse effect is found for the secondary velocity profiles. Also the temperature boundary layer thickness is decreased due to increase of Grashof number.

The primary velocity profiles and primary shear stress are increased due to increase of modified Grashof number where as the reverse effect is found for the secondary velocity profiles. Also the concentration boundary layer thickness is decreased due to increase of modified Grashof number.

The primary velocity profiles are increased due to increase of Prandtl number. The thermal boundary layer thickness as well as the heat transfer rate at the plate is decreased as the Prandtl number increases.

The heat transfer rate at the plate as well as the primary velocity is increased due to increase of Eckert number.

The temperature boundary layer thickness as well as the heat transfer rate at the plate is increased due to increase of thermal conductivity parameter.

The heat transfer rate at the plate is increased due to increase of heat source parameter.

The heat transfer rate at the plate is increased due to increase of radiation parameter.

The concentration boundary layer thickness as well as the mass transfer rate at the plate is decreased due to increase of Schmidt number.

The concentration boundary layer thickness as well as the mass transfer rate at the plate is decreased due to no reaction and destructive reaction.

The mass transfer rate at the plate is increased due to increase of order of chemical reaction.

COMPETING INTERESTS

Authors have declared that no competing interests exist.

REFERENCES

1. Bluman GW, Kumei S. Symmetries and Differential Equations. Springer-verlag: New York; 1989.
2. Helmy KA. MHD boundary layer equations for power law fluids with variable electric conductivity. *Mechanica*. 1995;30:187-200.
3. Pakdemirli M, Yurusoy M. Similarity transformations for partial differential equations. *SIAM Review*. 1998;40:96-101.

- 612 4. Kalpakides VK, Balassas KB. Symmetry groups and similarity solutions for a free
613 convective boundary-layer problem. *International Journal of Non-Linear Mechanics*.
614 2004;39:1659-1670.
- 615 5. Makinde OD. Free convection flow with thermal radiation and mass transfer past moving
616 vertical porous plate. *International Communications in Heat and Mass Transfer*. 2005
617 ;32:1411-1419.
- 618 6. Seddeek MA, Salem AM. Laminar mixed convection adjacent to vertical continuously
619 stretching sheet with variable viscosity and variable thermal diffusivity. *Heat and Mass*
620 *Transfer*. 2005;41:1048-1055.
- 621 7. Ibrahim FS, Elaiw AM, Bakr AA. Effect of the chemical reaction and radiation absorption
622 on the unsteady MHD free convection flow past a semi infinite vertical permeable
623 moving plate with heat source and suction. *Communications in Nonlinear Science and*
624 *Numerical Simulation*. 2008; 13:1056-1066.
- 625 8. El-Kabeir SMM, El-Hakiem MA, Rashad. Lie group analysis of unsteady MHD three
626 dimensional dimensional by natural convection from an inclined stretching surface
627 saturated porous medium. *Journal of Computational and Applied Mathematics*.
628 2008;213:582-603.
- 629 9. Rajeswari R, Jothiram J, Nelson VK. Chemical Reaction, Heat and Mass Transfer on
630 Nonlinear MHD Boundary Layer Flow through a Vertical Porous Surface in the Presence
631 of Suction. *Applied Mathematical Sciences*. 2009;3:2469-2480.
- 632 10. Chandrakala P. Chemical Reaction Effects on MHD Flow Past An Impulsively Started
633 Semi-Infinite Vertical Plate. *International Journal of Dynamics of Fluids*. 2010;6:77-79.
- 634 11. Joneidi AA, Domairry G, Balaelahi M. Analytical treatment of MHD free convective flow
635 and mass transfer over a stretching sheet with chemical reaction. *Journal of the Taiwan*
636 *Institute of Chemical Engineers*. 2010;41: 35-43.
- 637 12. Muhaimin, Kandasamy R, Hashim I. Effect of chemical reaction, heat and mass transfer
638 on nonlinear boundary layer past a porous shrinking sheet in the presence of suction.
639 *Nuclear Engineering and Design*. 2010;240(5):933-939.
- 640 13. Rahman MM, Salahuddin KM. Study of hydromagnetic heat and mass transfer flow over
641 an inclined heated surface with variable viscosity and electric conductivity.
642 *Communications in Nonlinear Science and Numerical Simulation*. 2010;15:2073-2085.